3D finite element simulation of the matter flow by surface diffusion using a level set method

Julien Bruchon, Sylvain Drapier, François Valdivieso

3D finite element simulation of the matter flow by surface diffusion using a level set method

J. Bruchon[1,*,†], S. Drapier[1] and F. Valdivieso[2]

[1]*LTDS CNRS UMR 5513, France*
[2]*PECM CNRS UMR 5146, Ecole des Mines de Saint-Étienne, Centre Sciences des Matériaux et des Structures, 7 158 cours Fauriel—42023 Saint-Étienne—Cedex 2, France*

Within the context of the sintering process simulation, this paper proposes a numerical strategy for the direct simulation of the matter transport by surface diffusion, in two and three dimensions. The level set formulation of the surface diffusion problem is first established. The resulting equations are solved by using a finite element method. A stabilization technique is then introduced, in order to avoid the spurious oscillations of the grain boundary that are a consequence of the dependence of the surface velocity on the fourth-order derivative of the level set function. The convergence and the accuracy of this approach are proved by investigating the change in an elliptic interface under surface diffusion. Cases in direct relation with the sintering process are analyzed besides: sintering between two grains of the same size or of two different sizes. Finally, 3D simulations involving a small number of particles show the ability of the proposed strategy to deal with strong deformations of the grain surface (formation of necks) and to access directly important parameters such as the closed porosity rate.

KEY WORDS: surface diffusion; level set method; sintering; curvature; Laplace-Beltrami operator

1. INTRODUCTION

Sintering process is a heating stage consisting of the consolidation of a metal or ceramic powder compact, which leads to a desired microstructure. During this stage, due to external or inner surface stress (curvature for the free sintering), necks are formed between particles by atom diffusion (see Figure 1). This consolidation can be achieved with or without reduction of porosity, depending on the transport paths of the matter. Roughly speaking, the sketch of a free sintering process in a solid state can be drawn as following (Figure 1). First, in order to reduce the surface energy, the matter flows over the grain free surface toward the minimum of curvature, i.e. toward the neck. This corresponds to the transport by surface diffusion. Owing to the neck formation, stress gradients appear in the material, giving rise to the grain boundary diffusion and consequently to the volume diffusion (see [1, 2]).

The general context of this work is the simulation of a sintering process, in a solid state and at a mesoscopic scale, that is, the direct simulation of the thermo-activated changes in metal or ceramic grains during a sintering process, including the different transport paths mentioned above. This paper describes the first step of this work, focusing on the simulation of the matter flow by

*Correspondence to: J. Bruchon, Ecole des Mines de Saint-Étienne, Centre Sciences des Matériaux et des Structures, 7 158 cours Fauriel—42023 Saint-Étienne—Cedex 2, France.
†E-mail: bruchon@emse.fr

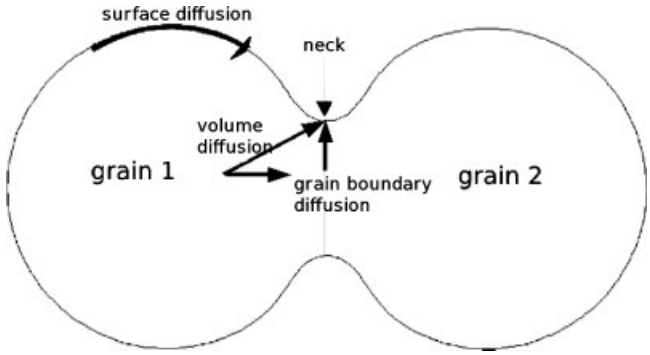

Figure 1. Different paths of matter flow between two grains.

surface diffusion. However, this general context has always to be kept in mind: it justifies why the numerical methodology presented here is not limited to a surface description of the grains (sufficient to deal with the surface diffusion), but adopts a more general volume representation.

The surface diffusion phenomenon results in a motion of the surface with a normal velocity, which is given by the Laplacian of its mean curvature. Such a motion has widely been studied from a mathematical standpoint (see for example [3, 4] for problems related to the shape stability). This flow preserves the volume enclosed inside the surface while minimizing its surface area. Furthermore, the evolution equation associated with this flow is a fourth-order equation, which leads to difficulties and instabilities when considering approximation techniques. Numerous papers developing numerical methods for the simulation of surface motion under Laplacian of curvature can be found in the literature, either in the specific sintering context [5–8] or in a more general context [9, 10]. The numerical strategies developed in these papers use finite difference or finite element approximations, and are based on a Lagrangian approach: a surface is described by a subset of the mesh boundary. However, despite the good results obtained in [10], the Lagrangian approach presents many difficulties, due to the sensitivity to the fourth-order derivatives of the position vector. Furthermore, such an approach cannot take into account naturally the topological changes that occurs during the flow by surface diffusion. In a sintering process, such topological changes occur when necks are created between grains, or when closed porosity is formed.

To overcome these difficulties, methods based on an Eulerian description of the surface have been investigated in the last two decades [11–14]. More precisely, these methods are based on the level set approach [15] that consists of embedding the surface in a higher dimensional function. The advantage of this technique is that topological changes are handled naturally. Metric properties of the surface (normal vector, curvature) can then be 'easily' deduced from this level set function [16, 17]. This point is very interesting when considering surface diffusion problems.

This paper presents a level set approach to deal with the flow induced by surface diffusion, using a finite element strategy. This point constitutes a first originality, since the above references using a level set approach are based on finite difference techniques. Once again, the reason of this choice is the general sintering simulation context, and the perspective to couple surface diffusion and mechanical computation. Another originality of this work is the decoupling between the computation of the normal velocity and the transport of the level set function. This may be considered as an 'engineering' point of view. The aim is to compute the normal velocity as an input data of a level set solver that is considered as a black box in a finite element code. The difficulty is that a straightforward scheme leads to spurious oscillations in the level set function.

This paper is organized as follows. Section 2 introduces the physical model and establishes, in a general framework, the equation of the surface diffusion. Section 3 details the numerical strategy developed to solve the surface diffusion problem. The level set description of the grains is introduced, and the variational formulation of the problem is written in a level set way. This formulation involves a dependence of the surface velocity on the fourth-order derivative of the distance function, leading to stability issues. These difficulties are overcame by considering a 'regularized' formulation. Finally, various numerical simulations are analyzed in Section 4, ranging

from an academic case involving an elliptic grain, to the sintering between two, five, and eight grains, in two and three dimensions.

2. PHYSICAL MODEL

Let Ω_g be a set of grains, and let S_g be the free surface of this set, as shown in Figure 2. Following the literature about ceramic sintering process modeling (see [1] and [2, Chapter 7]), the matter flow by surface diffusion is characterized by a flux $\mathbf{j_s}$ along the free surface S_g, driven by chemical potential gradients. In turn, these gradients depend on the gradient of the surface mean curvature K. Consequently, the surface flux can be expressed by

$$\mathbf{j_s} = -\frac{\delta_s D_s \Omega \gamma_s}{kT} \nabla_s K \tag{1}$$

where T is the absolute temperature, k is the Boltzmann's constant, D_s is the surface diffusion coefficient, δ_s is the thickness in which the diffusion occurs, γ_s is the surface free energy, and finally Ω is the molar volume of the material. In expression (1), operator ∇_s denotes the surface gradient, defined as the tangential component of the gradient

$$\nabla_s K = \nabla K - (\nabla K \cdot \mathbf{n})\mathbf{n}$$

where $\mathbf{n}$ is the outward-pointing unit vector normal to the free surface S_g (Figure 2). The surface gradient can easily be rewritten by introducing P, the projection matrix onto the tangent plane to S_g

$$\nabla_s K = P \nabla K$$

with

$$P = I - \mathbf{n} \otimes \mathbf{n} \tag{2}$$

where I is the identity matrix. Of course, the success of our numerical strategy will strongly depend on the good approximation of this projection matrix P.

The surface flux $\mathbf{j_s}$ results in the deposition or removal of material, which gives rise to a displacement rate, assumed to be normal to the surface. This surface diffusion velocity is then written as $\mathbf{v_s} = v_n \mathbf{n}$. The mass balance between, on one hand the matter which flows through the boundary of an elementary surface $S \subset S_g$ (see Figure 2), and on the other hand the displacement of this surface, is expressed by the relation

$$\int_{\partial S} \mathbf{j_s} \cdot \mathbf{n}_l \, \mathrm{d}l = -\int_S \mathbf{v_s} \cdot \mathbf{n} \, \mathrm{d}S \tag{3}$$

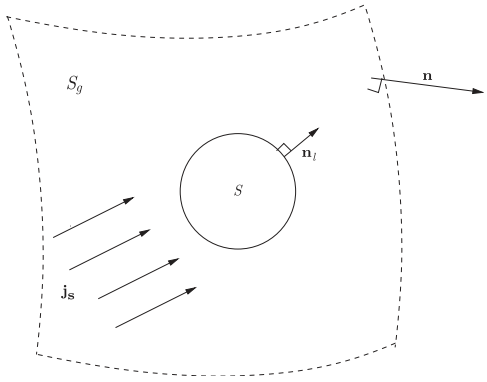

Figure 2. An elementary surface S of the grain free surface.

where $\mathbf{n}_l$ is the outward-pointing unit vector normal to ∂S (i.e. $\mathbf{n}_l$ belongs to the plane tangent to S depicted in Figure 2). By the divergence theorem, expression (3) is equivalent to

$$\int_S [\nabla_s \cdot \mathbf{j_s} + (v_n \mathbf{n}) \cdot \mathbf{n}] \, \mathrm{d}S = 0 \tag{4}$$

where $\nabla_s \cdot$ is the surface divergence operator. Since Equation (4) holds for any arbitrary surface $S \subset S_g$, the integrand is identically equal to zero. Consequently, the surface diffusion displacement rate is expressed by

$$\mathbf{v_s} = -(\nabla_s \cdot \mathbf{j_s})\mathbf{n} = C_0(\Delta_s K)\mathbf{n} \tag{5}$$

using Equation (1) with $C_0 = \delta_s D_s \Omega \gamma_s / kT$. The operator Δ_s, the 'surface Laplacian' operator is the so-called Laplace–Beltrami operator.

Before detailing the numerical method developed to discretize Equation (5), some key points have to be outlined. First, note that all the physical parameters involved in the description of the surface diffusion phenomenon, are contained into the parameter C_0. In all the simulations presented in this paper, C_0 is assumed to be constant into the computational domain. More precisely, the temperature will be considered as a constant, which means that only isothermal cases will be investigated. Second, it is well known in the sintering literature (see [2]) that the transport of matter by surface diffusion does not lead to shrinkage phenomena, that is, the distance between the grain centers remains constant under the flow. Furthermore, it is easy to show that the surface velocity given by Equation (5) preserves the volume. Indeed, if $|\Omega_g|$ is the grain volume measure, its variation during the process is expressed by

$$\frac{\mathrm{d}|\Omega_g|}{\mathrm{d}t} = \int_{S_g} \mathbf{v_s} \cdot \mathbf{n} \, \mathrm{d}S = \int_{S_g} \nabla_s \cdot \mathbf{j_s} \, \mathrm{d}S$$

Hence, since the flux is differentiable and S_g is a closed surface, $\mathrm{d}|\Omega_g|/\mathrm{d}t = 0$. Consequently, the grain volume remains constant. This point, as well as the absence of shrinkage, will be the criteria to assert the relevancy of our simulations.

3. NUMERICAL STRATEGY

3.1. Level set formulation

Let us consider a computational domain $\Omega \subset \mathbb{R}^d$, the unit square (spatial dimension $d = 2$) or the unit cube ($d = 3$). The grains evolve into this domain with respect to the velocity given by Equation (5), and are described by using the level set method introduced in [18], and applied in different contexts in [19] and [17]. More precisely, and without detailing this method, a smooth function $\phi : \Omega \times \mathbb{R}^+ \mapsto \mathbb{R}$ is introduced in the following way:

- At the initial time $t = 0$, ϕ is initialized by

$$\phi(x, t=0) = \begin{cases} \dfrac{2E}{\pi} \sin\left(\dfrac{\pi}{2E} d_0(x)\right) & \text{if } d_0(x) \in [-E, E] \\ -\dfrac{2E}{\pi} & \text{if } d_0(x) \leqslant -E \\ \dfrac{2E}{\pi} & \text{if } d_0(x) \geqslant +E \end{cases} \tag{6}$$

  where $d_0(x)$ is the initial signed distance from a point x to the grain free surface (d_0 is positive into the grains, negative outside, and is equal to zero along the free surface). Note that this distance function has to be computed only one time per simulation, during the initialization step, and that in the case of grains being initially spherical, this computation is very easy. The parameter E represents the interface 'width'. As $\sin(x) \approx x$ when $|x| \ll 1$, the above definition

means simply that $\phi(x,t)$ is equal to the signed distance function in a neighborhood of the grain free surface, while it is extended by a constant value (positive or negative) outside this neighborhood. The sine allows ϕ to be smooth through the surface $\{|d_0(x)| = E\}$.

- At a time t, knowing the transport velocity $\mathbf{v_s}(t)$ defined by Equation (5) in the vicinity of the free surface and extended to the whole computational domain Ω (by a way shown in the following), function ϕ is computed at time $t+\Delta t$, with Δt the time step, by solving a transport equation of the form

$$\frac{\partial \phi}{\partial t} + \mathbf{v_s} \cdot \nabla \phi = 0 \tag{7}$$

Classically (see [15]), even if function ϕ is initially a signed distance function (at least locally), this property which ensures its smoothness is not preserved by the transport step when an arbitrary velocity is used. Hence, an additional step, called reinitialization step, is usually required to recover this property without perturbing the interface. The originality of the level set method used in this work is to combine the transport step and the reinitialization step into a single convective reinitialization step, which preserves property (6). Consequently, transport equation (7) is modified in order to take into account the reinitialization of the level set function ϕ, 'far' from the isovalue zero. Further details can be found in [17–19].

We have to outline that with this method, as with any level set method, the interface, i.e. the grain free boundary, is characterized by the zero level set of ϕ. By definition, the value of $\phi(x,t)$ gives the position of a point x (e.g. a node of the mesh) at a time t with respect to the interface. Furthermore, and it is a key point for the surface diffusion simulation, the unit vector $\mathbf{n}_\phi$ normal to the interface and the mean curvature K_ϕ of this interface, can be expressed in a level set way by the two following relations (see [15, 16]):

$$\mathbf{n}_\phi = \frac{\nabla \phi}{\|\nabla \phi\|} \tag{8}$$

and

$$K_\phi = \nabla \cdot \frac{\nabla \phi}{\|\nabla \phi\|} \tag{9}$$

where $\|\cdot\|$ denotes the Euclidian norm in $\mathbb{R}^d$. Hence, if the level set function is known, then the curvature can be calculated, at least theoretically. Note that expressions (8) and (9) define the normal vector and the mean curvature in all the computational domain Ω, and not only over the free surface $\{\phi = 0\}$. Of course, parameters $\mathbf{n}_\phi$ and K_ϕ vanish outside the narrow band $[-E, E]$ around the interface, while they correspond to the usual normal vector $\mathbf{n}$ and curvature K in the vicinity of the interface (see [17]). Following [20], the surface diffusion velocity (5) can be rewritten in a level set form as

$$\mathbf{v_s} = v_n \frac{\nabla \phi}{\|\nabla \phi\|} \tag{10}$$

and

$$v_n = C_0 \frac{1}{\|\nabla \phi\|} \nabla \cdot (\|\nabla \phi\| P_\phi \nabla K_\phi) \tag{11}$$

where the projection matrix is now defined by

$$P_\phi = I - \frac{\nabla \phi}{\|\nabla \phi\|} \otimes \frac{\nabla \phi}{\|\nabla \phi\|}$$

Velocity (10) is defined in the whole computational domain, and corresponds, in the vicinity of the zero level set of ϕ, to the surface diffusion velocity. The differential operators (gradient and divergence) involved in Equation (11) are now expressed explicitly with the Cartesian coordinates (x, y, z), and can therefore be computed within the context of an Eulerian description of the grains.

3.2. Finite element discretization

Formulation (11) is discretized by using a finite element approach. Hence, let the computational domain $\Omega \subset \mathbb{R}^d$ be discretized by a simplex mesh $\mathscr{T}_h(\Omega)$. An element $e \in \mathscr{T}_h(\Omega)$ is a triangle if $d=2$, and a tetrahedron if $d=3$. The unknowns ϕ, K and v_n are approximated by ϕ_h, K_h and v_{nh}, respectively, chosen as being continuous and piecewise linear over Ω. Furthermore, the partition $0=t_0<t_1<\cdots<t_\Theta=\Theta$ of the time interval $[0,\Theta]$ is introduced. A field X evaluated at the time t is then denoted by X^t.

Regarding Section 3.1, all seems easy: if ϕ_h^t is assumed to be known, then K_h^t and ${v_n}_h^t$ can be computed by using the variational forms of (8), (9), and (11). However, two difficulties appear and must be clearly understood. First, the velocity v_{nh} depends on the fourth-order spatial derivative of ϕ_h. Since ϕ_h is piecewise linear, the gradient $\nabla\phi_h$ is piecewise constant, and $\nabla^{(n)}\phi_h \equiv 0$ when $n \geqslant 2$. Equations (9) and (11) must therefore be considered in a weak sense, as in [20, 21]. The second difficulty is the nonlinear coupling between the level set function ϕ, the curvature and the surface diffusion velocity. At this point, we have to mention that within the general context of this work, the simulation of the sintering processes, expression (11) represents only the first contribution to the 'global' sintering velocity, which is the sum of the displacement rates involved by the different paths of matter transport. Consequently, in order not to develop a numerical method which would be dedicated only to the surface diffusion, velocity is treated in an explicit way in the transport equation (7). In other words, $\phi_h^{t+\Delta t}$ is computed by solving Equation (7) with the velocity $\mathbf{v}_{\mathbf{s}_h}^t$, i.e. evaluated on the configuration corresponding to ϕ_h^t (see Section 3.3).

3.2.1. A fully explicit formulation. The first approach for solving system (7)–(9) and (11) is to solve each equation successively in an explicit way. Furthermore, additional diffusion terms $\varepsilon_K \Delta K$ and $\varepsilon_v \Delta v_n$ are then considered in the left-hand side of Equations (9) and (11), respectively (elliptic regularization, see [22]), where ε_K and ε_v are two numerical parameters. The regularization effect of the term $\varepsilon_K \Delta K$ is shown in Figure 3. In this example ϕ_h is the distance to the circle of radius $R=0.2$. The curvature K_h is calculated by using the regularized weak form of (9)

$$\int_\Omega K_h \psi_h \,\mathrm{d}\Omega + \varepsilon_K \int_\Omega \nabla K_h \cdot \nabla \psi_h \,\mathrm{d}\Omega = -\int_\Omega \frac{\nabla \phi_h}{\|\nabla \phi_h\|} \cdot \nabla \psi_h \,\mathrm{d}\Omega$$

for all test functions ψ_h continuous and piecewise linear on Ω. K_h is therefore a field defined in each point of the computational volume, and should be equal to the circle curvature ($K=5$) in the vicinity of the level set $\{\phi_h=0\}$. When no regularization is considered ($\varepsilon_K=0$) as in Figure 3(a), the level set $\{K_h=5\}$ is shown to be scattered in a wide band around the interface. Clearly, the curvature is not computed with accuracy. However, if a small diffusion parameter is considered ($\varepsilon_K=10^{-4}$ in Figure 3(b)), the level sets $\{\phi_h=0\}$ and $\{K_h=5\}$ are perfectly superimposed, showing the accuracy of the curvature computation. Note that an additional level set $\{K_h=5\}$ appears inside the grain. This second level set corresponds to a discontinuity of the second-order derivative of

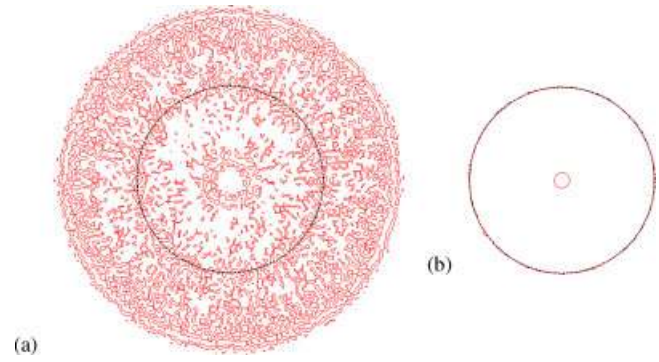

Figure 3. Level set $\{\phi_h=0\}$ (circle of radius $R=0.2$, black line), and level set $\{K_h=5=1/R\}$: influence of the regularization parameter ε_K. (a) $\varepsilon_K=0$ and (b) $\varepsilon_K=10^{-4}$.

ϕ_h, induced by the extension of ϕ_h by a constant value. However, this discontinuity is far from the interface and does not disturb its motion.

This example shows clearly that introducing a regularization parameter is necessary for the curvature computation. Nevertheless, the regularization of Equation (11) is shown to be much more complex: if ε_v is too 'large' (with respect to the values of the velocity), the solution is stable but the computed velocity is underestimated (see Section 4.1). In contrast, taking a 'small' value of ε_v leads to an accurate computation of the velocity in the early steps of the simulation, before giving rise to spurious oscillations of the interface as shown in Figure 4. Although these oscillations can be prevented by using a 'small' time step, this unstable behavior, and the two additional numerical parameters introduced, encourage us to develop the more implicit and stable formulation presented in the following section.

3.2.2. A mixed $K/\Delta_s K$ formulation. Assuming that ϕ_h^t is known (at a time t), the numerical method proposed in this section consists of building a system, the unknowns of which are the curvature K_h^t and the normal velocity ${v_n}_h^t$ (which is equal to $C_0\Delta_s K_h$ regarding Equation (5)). In order to introduce implicitly a regularization term in this formulation, the following first-order Taylor's expansion is considered:

$$\phi_h^{t+\frac{1}{2}} \underset{def.}{=} \phi_h^t + \frac{\partial \phi_h^t}{\partial t}\Delta t = \phi_h^{t+\Delta t} + o(\Delta t)$$

Hence, $\phi_h^{t+\frac{1}{2}}$ is a first-order approximation of $\phi_h^{t+\Delta t}$. Since the level set function ϕ is solution of the transport equation (7), $\partial\phi/\partial t = -\mathbf{v_s}\cdot\nabla\phi$, and the previous relation can be turned into

$$\phi_h^{t+\frac{1}{2}} = \phi_h^t - \mathbf{v_s}_h^t \cdot \nabla\phi_h^t \Delta t$$

Finally, since $\nabla\phi_h^t \cdot \nabla\phi_h^t = \|\nabla\phi_h^t\|^2$, taking into account expression (10) of the velocity leads to

$$\phi_h^{t+\frac{1}{2}} = \phi_h^t - {v_n}_h^t \|\nabla\phi_h^t\| \Delta t \tag{12}$$

The system with unknowns K and $\Delta_s K$ can now be constructed by considering $\phi_h^{t+\frac{1}{2}}$ instead of ϕ_h^t in relation (9) giving the curvature of the discretized level set function. Hence, at a time t, assuming that ϕ_h^t is known, the system to be solved for both curvature K_h^t and normal velocity ${v_n}_h^t$, is given by

$$\begin{aligned} K_h^t + \nabla\cdot\left(\frac{\Delta t}{A}\nabla {v_n}_h^t\right) &= \nabla\cdot\left(\frac{1}{A}\nabla\phi_h^t\right) \\ {v_n}_h^t\|\nabla\phi_h^t\| - C_0\nabla\cdot(\|\nabla\phi_h^t\| P_{\phi_h^t}\nabla K_h^t) &= 0 \end{aligned} \tag{13}$$

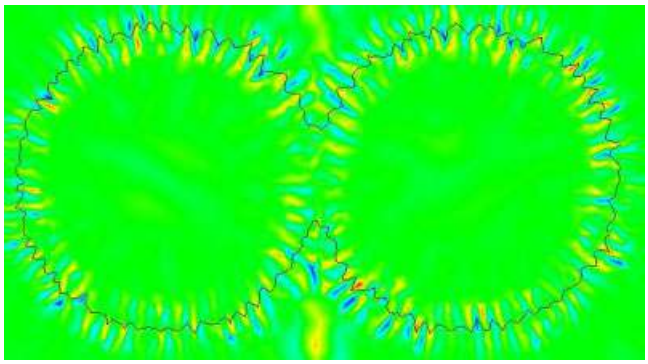

Figure 4. Zero level set of the level set function (grain surface, black line) and isovalues of the curvature (alternatively negative and positive), in an unstable case $\varepsilon_v = \varepsilon_K = 10^{-4}$.

Since ϕ is a distance function in the vicinity of the interface $\{\phi=0\}$, $\|\nabla\phi_h\|$ is approximatively equal to 1 near this interface. This is why $\|\nabla\phi_h\|$ does not appear in the second term of the first equation of (13) (we will see that this term is only a regularization term). Furthermore, the term denoted by A in this equation is normally equal to $\|\nabla\phi_h^{t+\frac{1}{2}}\|$. However, to avoid to deal with this nonlinear term, the computations presented in this paper have been performed by doing the approximation $A=\|\nabla\phi_h^t-\Delta t\nabla {v_n}_h^{t-\Delta t}\|$.

The key point of this approach is that using $\phi_h^{t+\frac{1}{2}}$ instead of ϕ_h to compute the curvature induces an additional term in the left-hand side of the first equation of (13). This K/v_n coupling term is equivalent to a regularization term Δv_{nh} with the regularization parameter $\Delta t/A$. Hence, unlike the previous fully explicit formulation, only one regularization term is necessary to compute the curvature and the surface diffusion velocity. Furthermore, the corresponding regularization parameter appears naturally and depends on the time step only.

Formulation (13) shows strong similarities with the one developed by Bänsch within the context of a Lagrangian description of the particles [21]. The stability of this formulation will be not mathematically established in this paper, contrary to [21]. However, the good behavior of (13) is shown through various simulations.

Finally, the effective computation of K_h and v_{nh} is carried out by considering the finite element discretization of (13). As previously, a simplex mesh on Ω is considered, while ϕ_h, K_h, and v_{nh} are chosen belonging to the space of continuous and piecewise linear functions on Ω, denoted $\mathscr{V}_h$. The mixed weak formulation of (13) is then written as: at time t, assuming ϕ_h^t known, find $(K_h^t, {v_n}_h^t)\in\mathscr{V}_h\times\mathscr{V}_h$ solution of

$$\begin{aligned}
&\int_\Omega K_h\psi_h\,\mathrm{d}\Omega-\Delta t\int_\Omega\frac{1}{A}\nabla {v_n}_h^t\cdot\nabla\psi_h\,\mathrm{d}\Omega=-\int_\Omega\frac{1}{A}\nabla\phi_h^t\cdot\nabla\psi_h\,\mathrm{d}\Omega\\
&\int_\Omega\|\nabla\phi_h^t\|{v_n}_h^t\psi_h\,\mathrm{d}\Omega+\int_\Omega C_0\|\nabla\phi_h^t\|(P_{\phi_h^t}\nabla K_h^t)\cdot\nabla\psi_h\,\mathrm{d}\Omega=0
\end{aligned}\tag{14}$$

for all $\psi_h\in\mathscr{V}_h$. Note that one single type of weighting functions ψ_h has been used for the curvature equation and for the velocity one, since both curvature and velocity belong to the same functional space $\mathscr{V}_h$. Furthermore, previous equation (14) does not require the enforcement of any Dirichlet condition: since ϕ_h is constant in the vicinity of $\partial\Omega$, K_h, and v_{nh} vanish over the domain boundary.

3.3. Time stepping strategy

The above developments are summarized by the following time-stepping strategy, adopted for the simulation of the matter flow by surface diffusion.

0. Given a computational domain Ω (the unit square or the unit cube) discretized with a fixed unstructured simplex mesh, achieve the initialization of the level set function ϕ_h at $t=0$ by Equation (6).
1. At time $t=t_n$, assuming ϕ_h^t is known, achieve
   (a) Mesh adaptation with respect to the level set function ϕ_h^t.
   (b) Computation of the normal surface diffusion velocity v_{nh} by solving system (13).
   (c) Computation of the surface diffusion velocity $\mathbf{v}_{\mathbf{s}h}$ by Equation (10).
   (d) Computation of $\phi_h^{t+\Delta t}$ by solving the transport equation (7) in its reinitialization-convection form.
2. $t_n\leftarrow t_{n+1}$. If $t_{n+1}<\Theta$ (the final time), back to step 1.

A remeshing step appears in the above scheme. This step is based on the metric properties of the level set function ϕ_h, and aims to improve the description of the interface $\{\phi_h=0\}$ by refining the mesh within the interface vicinity. In this way, the description of the interfaces is improved, while the CPU time cost is preserved. In the simulations presented in this paper, the mesh size is isotropic: a minimal mesh size $h_{\min}$ is imposed when $|\phi_h|\leqslant d_{\min}$, a maximal mesh size $h_{\max}$ is imposed when $|\phi_h|\geqslant d_{\max}$, and the mesh size is assumed to be continuous and linear between these

extrema. The above parameters $h_{\min}$, $h_{\max}$, $d_{\min}$, and $d_{\max}$ are defined by the user (they are not related to any error analysis). At each remeshing step, the level set function ϕ_h is projected from the 'old' mesh onto the new one by P1 interpolation. The influence of this projection is evaluated in Section 4. Further details can be found in [17].

4. NUMERICAL SIMULATIONS

This section presents several direct simulations of change in free surface by surface diffusion, using the numerical strategy developed previously. These simulations have been carried out by using the CIMLIB finite element library. This C++ library, which is highly parallel, is developed at the Centre de Mise en Forme des Matériaux (Mines ParisTech, CNRS UMR 7635) by Coupez and co-workers (see [18, 23, 24]).

First, based on a case proposed in [13], Figure 5 shows a star shape flowing under Laplacian of curvature. In this example, the star shape is composed of 3 ellipses with a ratio between the major and minor axes equal to 10. Parameter C_0 (Equation (5)) is taken equal to 2×10^{-3}, while the time step for this calculation is $\Delta t = 5\times10^{-4}$. The shape becomes roughly circular within 5000 iterations (Figure 5(d)). Furthermore, this case is used to evaluate the influence of the remeshing step on the calculation, that is, the influence of the amount of diffusion introduced by the P1 projection, on the evolution of the free surface. Hence, two simulations are compared in Figure 5. The first one, in dashed line in Figure 5, has been achieved by using an unstructured mesh with a uniform mesh size equal to 6.25×10^{-3}, and without mesh adaptation; the second simulation, in black solid line, uses the mesh adaptation strategy with a minimal mesh size of 6.25×10^{-3}, a maximal one equal to 8.0×10^{-2}, and a remeshing step applied every three time steps (which is a high remeshing frequency regarding the investigated case). The evolution of the star shape is shown to be similar in both cases. Hence, perturbation in the free surface evolution, due to the remeshing step, seems to be acceptable. In fact, the remeshing step works well when considering adaptation with respect to the distance function, because this function can be assumed to be nearly linear in the vicinity of the free surface (if this last one is smooth enough). In this case, P1 interpolation from mesh to mesh is then exact. Further finite element simulations involving very accurate descriptions of free surfaces with mesh adaptation can be found in [18].

4.1. Change in an ellipsoid interface by surface diffusion

The simulations presented in this section investigate the evolution of an ellipsoid shape under surface diffusion. This 'academic' case aims to assert the efficiency of the methodology presented in this paper by comparing the simulation results with an analytical model. The computational domain Ω is the unit square (two-dimensional case), and let d_0 (see Equation (6)) be the function defining the signed distance with respect to an oval shape. In the first time, and following [13], this case is used to verify the convergence and conservation properties of our method. Since the matter transport by surface diffusion tends to minimize the surface energy while preserving the volume, starting with a ratio between the major and minor axes equal to 4 (and using $C_0 = 2\times10^{-6}$, $\Delta t = 5\times10^{-4}$), the interface $\{\phi_h = 0\}$ adopts progressively a circular shape. This evolution will be discussed in more details in the following. Here, Figure 6 points out the convergence properties

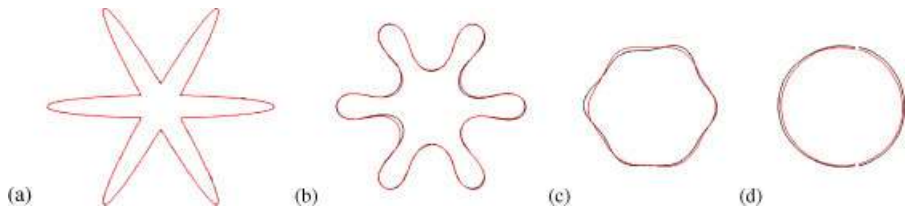

Figure 5. Evolution of star shape (at times $t = 0$, 0.3, 1.25, and 2.5): without mesh adaptation (black solid line) and with mesh adaptation (dashed line).

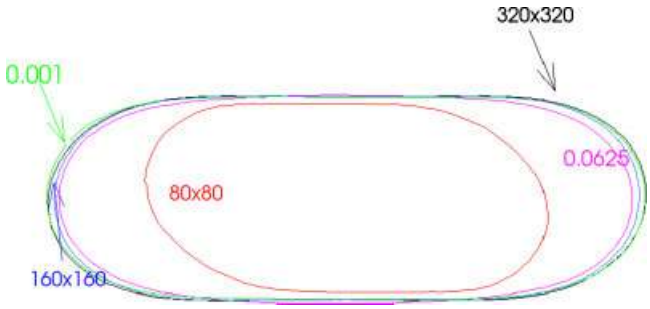

Figure 6. Computation of oval at time $t=2.5$ with different spatial resolutions (number of elements for structured mesh or (local) mesh size for unstructured mesh).

of our method by showing the zero level set of ϕ_h obtained after 5000 time steps with different space discretizations. Several structured meshes have been used (80×80, 160×160, and 320×320 meshes), as well as one unstructured meshes with a mesh size of 6.25×10^{-3} (which corresponds to the mesh size of the 160×160 mesh) and another one with a mesh size of 10^{-3}. Beside the convergence in shape, the convergence in the area conservation property can also be observed in Figure 6. The area loss is equal to 40, 2.8, and 0.9% of the initial area respectively for the three structured meshes, while it is equal to 2.4% for the unstructured mesh having a uniform mesh size of 6.25×10^{-3} (without mesh adaptation, 34 000 nodes), and to 6% when the remeshing technique is applied with $h_{\min}=6.25\times10^{-3}$ (approximatively 2200 nodes). However, when using the mesh adaptation method with $h_{\min}=10^{-3}$ (12 000 nodes), the area loss drops to 1%. Hence, to complete the previous section, even if the mesh adaptation introduces an additional numerical diffusion which can lead to a gain or loss in mass, the previous star shape (Figure 5) and oval shape (Figure 6) studies show that there are convergence in shape as well as in mass conservation when using a remeshing technique.

Next, we propose to analyze in more details the change of an ellipsoid shape in a circular shape under Laplacian of curvature. Figure 7 shows the simulation of this flow, for an ellipse of axes 0.3 and 0.2, performed by solving the mixed formulation (13) with the value $C_0=10^{-3}$. This parameter is constant and therefore acts as a scale parameter in space and time. The time step is $\Delta t=10^{-3}$, while the mesh size varies from 5.0×10^{-3} in the vicinity of the interface to 3.0×10^{-2} elsewhere. It can be verified in Figure 7 that the interface, represented by the line in bold, evolves toward a circular shape as expected. Furthermore, the curvature, which has its non-zero isovalues presented in Figures 7(a) and (b) in a narrow band around the interface, tends to become homogeneous and to converge toward the value $K_f=4.08$. This is the expected equilibrium value: the square of the corresponding radius $R_f=1/K_f=0.245$ is equal to 0.06, which is the value of the product between the initial minor and major axes. Hence, once again, the volume is well preserved during the simulation. Finally, the normal velocity obtained by solving system (13) is shown in Figure 7(c) at time $t=0$. As expected, the velocity is extremal where the variations of curvature are extremal.

Until now, only the final shape of the interface, that is the steady state, has been studied. However, it is possible to compare the interface position with the predictions provided by an analytical model all along the simulation. Let $a(t)$ and $b(t)$ be the major and minor axes of the ellipse at time t, with $a(0)=0.3$ and $b(0)=0.2$. The surface Laplacian of the ellipse curvature can 'easily' be calculated (for instance by using a symbolic computation software), and the velocity of the major axis (the point $(a(t),0)$) is given by

$$\mathbf{v_s}(a)=C_0\frac{3(b^2-a^2)a}{b^6}$$

Hence, at time $t+\Delta t$, a can be evaluated by an explicit Eulerian scheme, $a(t+\Delta t)=a(t)+\Delta t\mathbf{v_s}(a(t))$, while b is simply obtained by $b=a(0)b(0)/a$. Figure 8 presents a comparison over time between the values of a and b by three different ways: the analytical model, from the level set approach when system (13) is solved (red lines), and from the fully explicit formulation (blue lines, with $\varepsilon_v=\varepsilon_K=10^{-3}$ and still $\Delta t=10^{-3}$). The results provided by the mixed method show

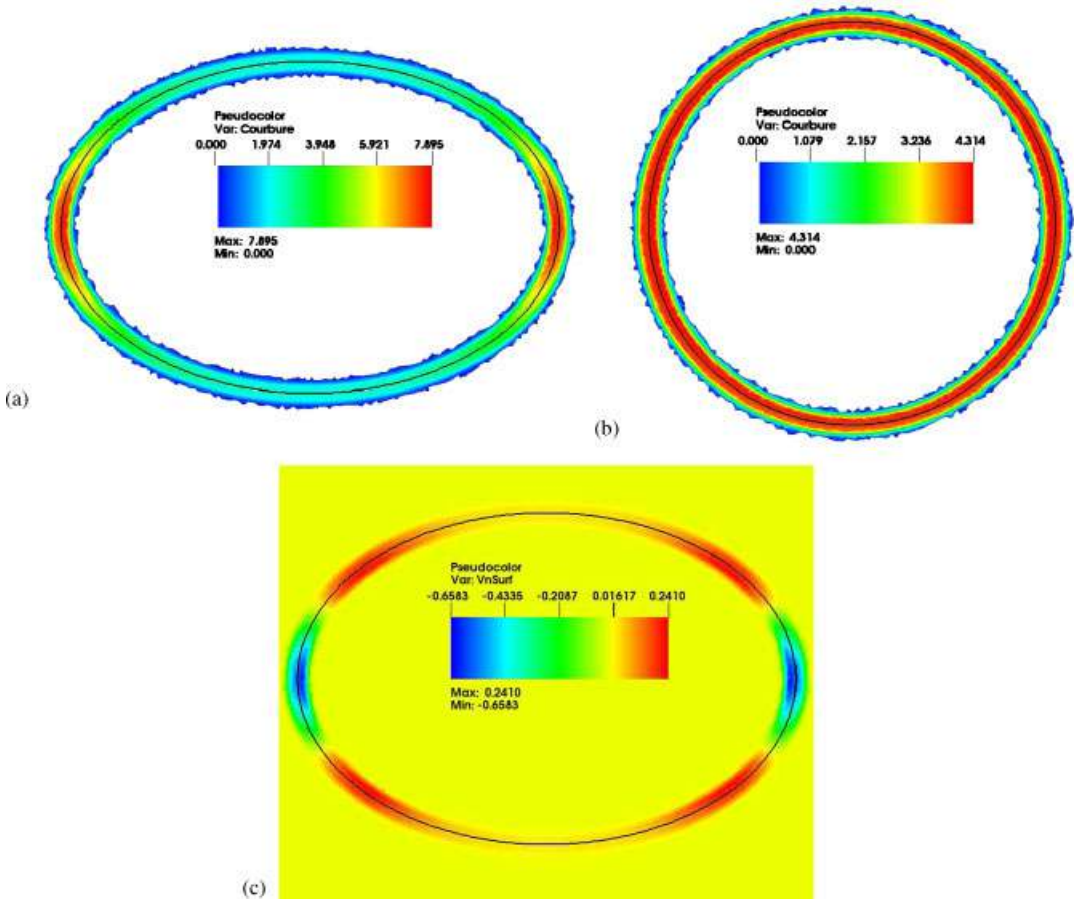

Figure 7. Change in the interface $\{\phi_h = 0\}$ (line in bold), initially an ellipse, toward a circular shape by surface diffusion. (a) Curvature at $t = 0$; (b) curvature at $t = 1$; and (c) normal velocity at $t = 0$.

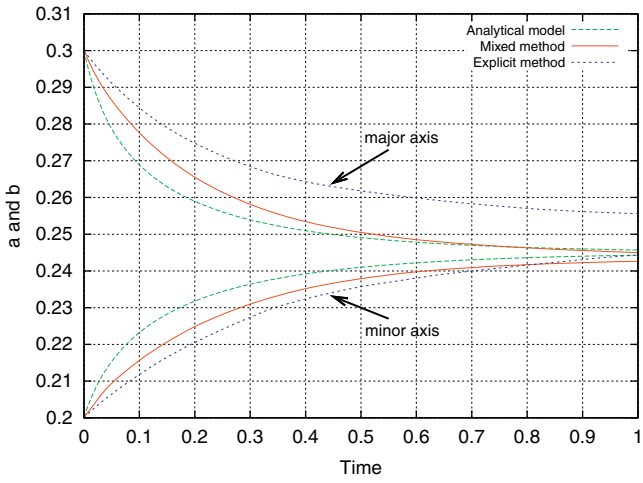

Figure 8. Change in the major and minor axes of the interface over time: analytical model, simulation with the mixed approach, and simulation with the fully explicit approach ($\varepsilon_v = \varepsilon_K = 10^{-3}$).

a good behavior of the interface, with a maximal error on both major and minor axes lower than 3%. The fully explicit method does not exhibit such a behavior, with an important error on the interface position. Furthermore, as already mentioned, this method appears to be unstable when, for

instance, $\varepsilon_v = \varepsilon_K = 10^{-4}$ and $\Delta t = 10^{-3}$, or when $\varepsilon_v = \varepsilon_K = 10^{-4}$ and $\Delta t = 10^{-4}$. Finally, note that 1000 time steps have been carried out with the mixed approach for a CPU time of approximatively 600 s on one processor of 2.2 GHz and with a mesh of approximatively 4800 nodes.

4.2. Change in two grains of the same size by surface diffusion

From this section, simulations in direct relation with sintering process are investigated. The first case involves two spherical grains of equal radii $R = 0.2$, as depicted in Figure 9. As in every simulation presented in this paper, one single level set function ϕ_h is used to represent the set of grains. This function is initialized at each mesh node, as the maximum of the level set functions associated with each spherical grain (because of the sign convention adopted in Equation (6)). As shown in Figure 9(a), the grains are initially nearly tangential. It has to be pointed out that there is no special algorithm to deal with either the contact surface or the singularities of the level set function that is not differentiable on the triple junction. However, despite the initial 'roughness' of the area of contact between the grains, and due to the matter diffusion, this area becomes quickly smooth as shown in Figure 9. This phenomenon is specifically outlined in Figure 10: the triple junction (contour of the contact surface) appears to be very irregular when the computation starts (its shape depends on the mesh size), while it has been greatly smoothed after only 10 time steps, and it has become a perfect circle within 20 increments. Furthermore, the flow under Laplacian of curvature has a physical meaning only if the curvature and its second-order derivatives exist, that is, only if the triple junction is smooth enough. Hence, this early stage of the simulation allows us to obtain a triple junction in a 'natural' and easy way. Our simulations and the study presented below prove that this stage does not affect the subsequent evolution of the grain cluster. Furthermore, the rate of change in grain volume is presented in Table I. Of course, this rate depends

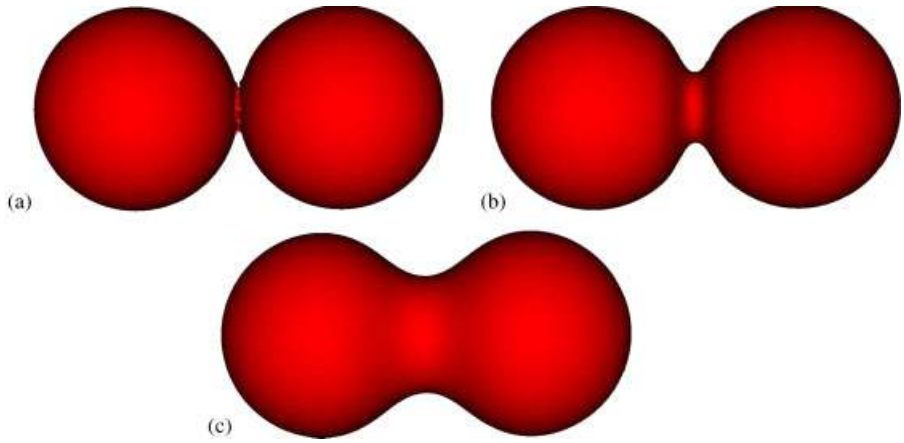

Figure 9. Change in the interface $\{\phi_h = 0\}$ during the sintering by surface diffusion between two grains of equal size (radius $R = 0.1$). (a) $t = 0$; (b) $t = 10^{-2}$; and (c) $t = 3$.

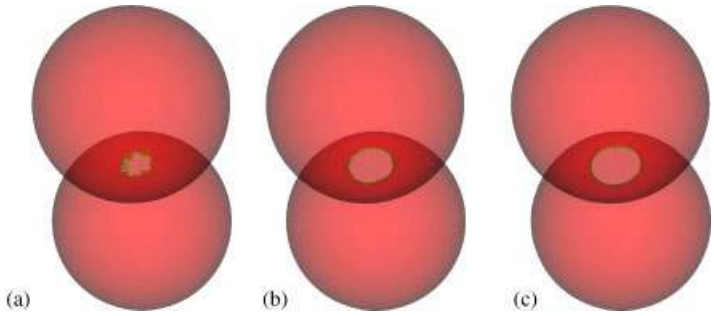

Figure 10. Triple junction (contour of the contact surface) at times $t = 0$, $t = 10^{-2}$ and $t = 2 \times 10^{-2}$, respectively.

on the mesh size (and on the time step) as studied previously. However, the values of Table I show that the formation of a neck between the grains (for a time $t<0.05$) does not change the grain volume. Here, the grain volume is well preserved, with a variation of 0.8% in 1000 increments. As expected, no shrinkage phenomenon occurs since the grain centers do not move.

The radius x of the circular contact area is called the neck radius. Theoretical models, based on geometrical assumptions and established within the context of sintering process modeling (see [2]), predict that the adimensional neck radius x/R behaves as the power $1/7$ of the time:

$$\frac{x(t)}{R}=\left(\frac{56C_0}{R^4}t\right)^{1/7}=1.78t'^{1/7} \tag{15}$$

where t' is an adimensional time, defined by $t'=(C_0/R^4)t$. Figure 11 shows, in logarithmic scales, the evolution of the adimensional radius x/R, obtained by direct simulation for different values of the grain radius, ranging from 0.1 to 2.5. As predicted by Equation (15), this evolution over t' does not depend on the grain radius R, and behaves as $t^{1/7}$. Hence, despite an initial contact surface between the grains which is not well defined as already mentioned, the radius x/R provided by each simulation tends quickly toward a same curve of the same form as (15). Instead of the coefficient 1.78 given by the analytical model, our simulations provide a coefficient equal to 1.3. The curves corresponding to these two values are denoted in Figure 11 by 'Analytical model, 1/7' and 'Simulation, 1/7', respectively. It has to be underlined that this result is shown to be stable with respect to the time step (ranging from 10^{-6} to 10^{-2}), with respect to the mesh size (ranging from 10^{-4} to 10^{-2}, with isotropic or anisotropic remeshing), and thus with respect to the initial neck radius: in all the investigated cases, the neck radius x/R obtained by direct simulation, tends quickly toward a 'master curve' of the type given in Equation (15) with a coefficient approximatively equal to 1.3. However, in Equation (15), the two key parameters that characterize the surface diffusion from the grain surface toward the neck, are, on one hand the power $1/7$, and on the other hand, the power 4 applied to R in the denominator (see [2]). The differences between the simulations and the analytical model can be explained by the geometrical approximations made in this latter.

Table I. Surface diffusion between two grains of radius $R=0.2$: rate of change in volume of grains ($C_0=10^{-6}$, $\Delta t=10^{-3}$, $h_{\min}=8.0\times10^{-3}$).

Time	0	0.02	0.06	0.1	0.4	0.6	1
Change (%)	0	+0.023	+0.0005	−0.011	−0.18	−0.44	−0.79

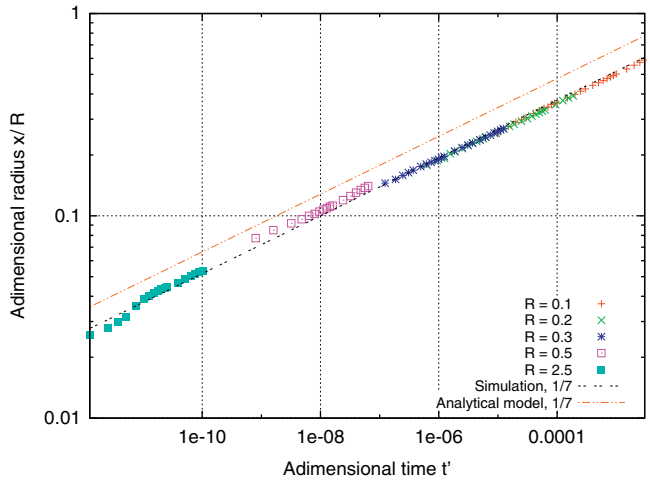

Figure 11. Change in the adimensional neck radius x/R over adimensional time t' (logarithmic scale) for different values of R, and with $C_0=10^{-7}$.

4.3. Change in two grains of different size by surface diffusion

A simulation involving two grains of different sizes ($R_1=0.1$ and $R_2=0.2$) is described in Figure 12. Except the size, exactly the same conditions as previously are considered. First of all, it has to be outlined that the grain centers do not move during the sintering by surface diffusion: there is no shrinkage. As the sizes of the two grains are different, the neck radius x cannot be considered *a priori* in a dimensionless form, and the evolution of x is directly plotted over time t in Figure 13. However, Pan *et al*. [25] and Martin *et al*. [26] propose to define an equivalent radius $\overline{R}$ by

$$\overline{R}=\frac{2R_1R_2}{R_1+R_2}$$

In the present case, the direct simulation permits us to show the relevancy of this definition. Indeed, the temporal change in the neck radius involved by two grains of the same radius $\overline{R}=0.1333$ (the equivalent radius for $R_1=0.1$, $R_2=0.2$) is also plotted in Figure 13. This change is shown to perfectly fit the one induced by the two grains of radii 0.1 and 0.2.

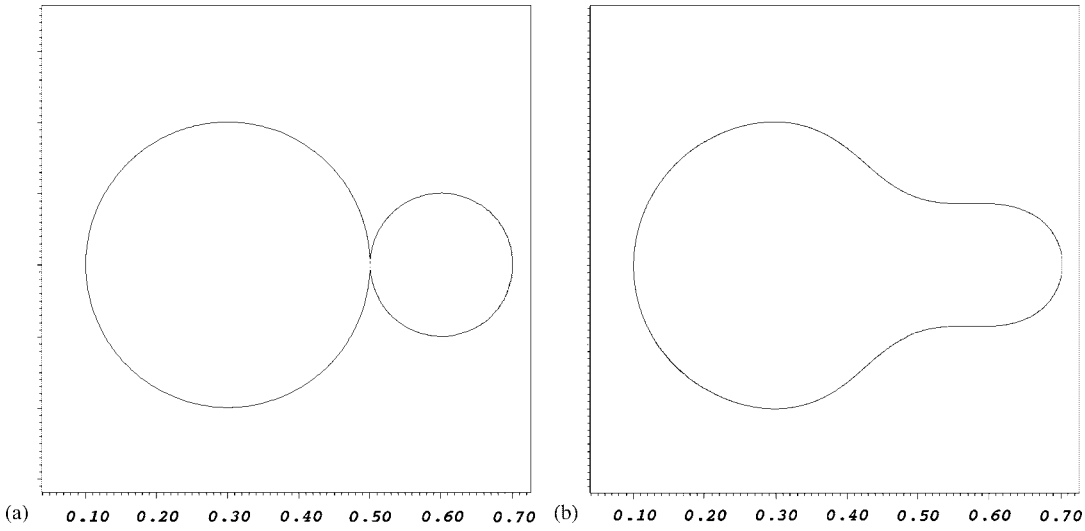

Figure 12. Change in the interface $\{\phi_h=0\}$ during the sintering by surface diffusion between two grains of different radii ($R=0.1$ and $R=0.2$). (a) $t=0$ and (b) $t>0$.

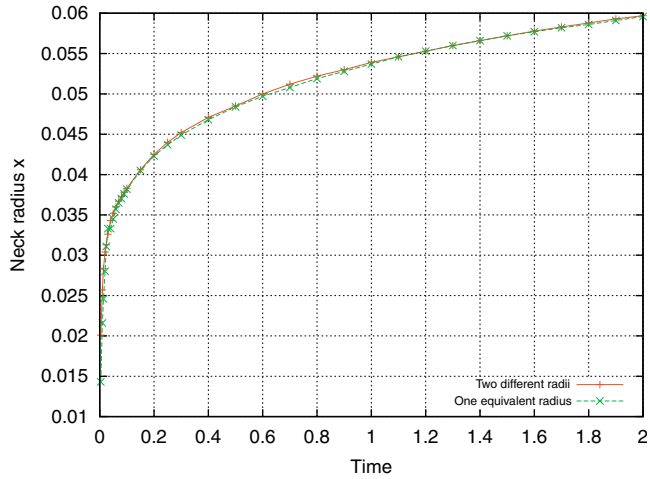

Figure 13. Temporal change in the neck radius x for two grains of different radii ($R_1=0.1$ and $R_2=0.2$) and for two grains of the same equivalent radius ($\overline{R}=0.133$).

4.4. Change in a small cluster of grains by surface diffusion

This section presents two simulations that involve a small cluster of grains. The first simulation deals with the sintering by surface diffusion of five grains disposed as in Figure 14. The key points of this two-dimensional simulation are as following. First, there is no shrinkage and the grain volumes are preserved during the simulation. Second, the neck formation and the evolution of the cluster toward a steady state by surface diffusion is clearly observed. Furthermore, a kind of closed porosity (in two dimensions) appears in this simulation. Hence, the numerical strategy based on a level set approach developed in this paper allows us to take into account automatically any complex topological change in the grain free surface, and then to have a direct access to parameters of first interest for the microstructure control, such as the porosity ratio. It has to be pointed out that the accuracy of the interface description is largely improved by the mesh adaptation strategy previously mentioned. For example, the adapted mesh at $t=0$ can be seen in Figure 14(a). The isovalues of the initial curvature defined by (13) are superimposed in this same figure. As expected, the curvature is extremal in the neck vicinity.

Finally, Figure 15 shows the temporal change, by surface diffusion, in eight grains in a three-dimensional configuration. The computational domain is the unit cube, discretized with an unstructured meshed made up of 350 000 tetrahedrons (60 000 nodes). The numerical strategy previously detailed and a mesh adaptation method are still considered. The parameter C_0 has been taken equal to 10^{-7}, while the time step is $\Delta t = 10^{-2}$. Neck formation is observed, and the cluster evolves

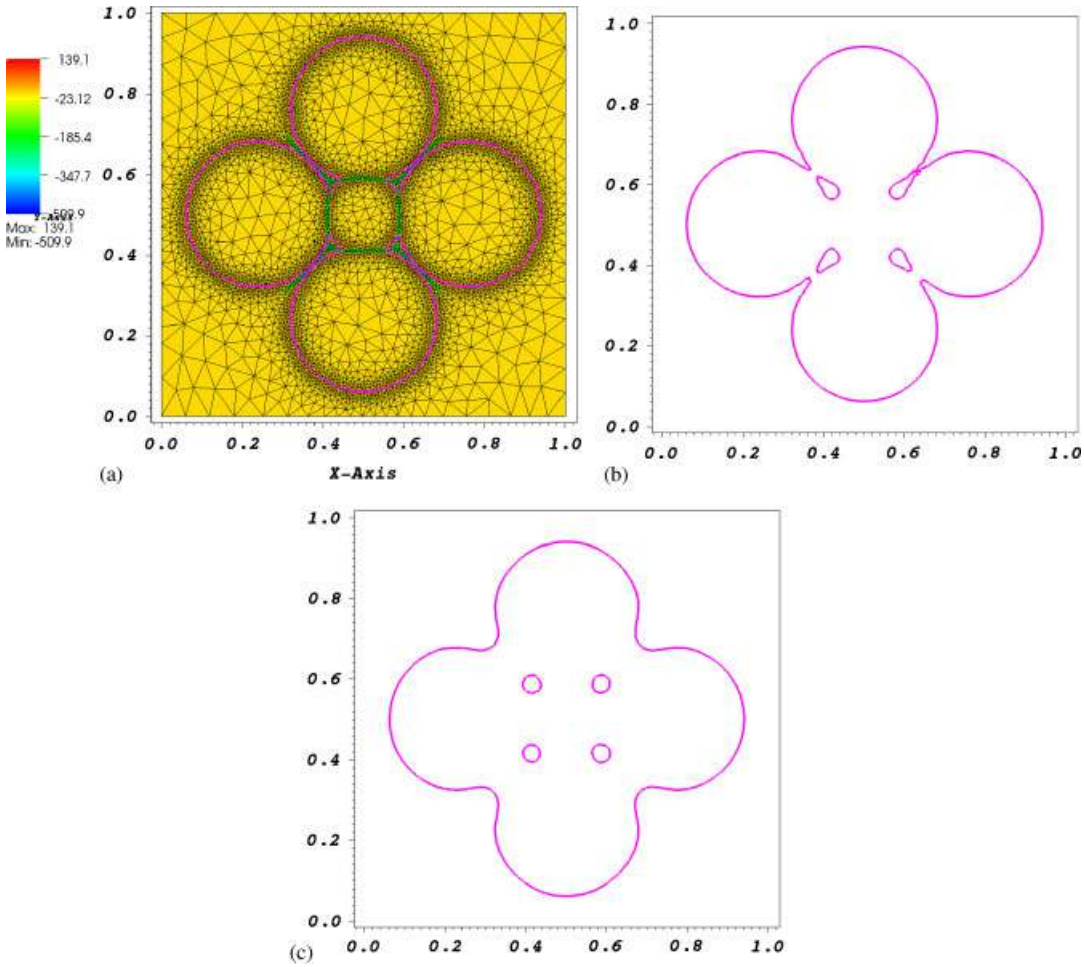

Figure 14. Change in 5 grains under surface diffusion (two-dimensional case, $C_0 = 10^{-7}$, $\Delta t = 5.0 \times 10^{-3}$). (a) Adapted mesh and curvature, and (a)–(c) Interface $\{\phi_h = 0\}$ (solid line). (a) $t=0$; (b) $t=0.1$; and (c) $t=5$.

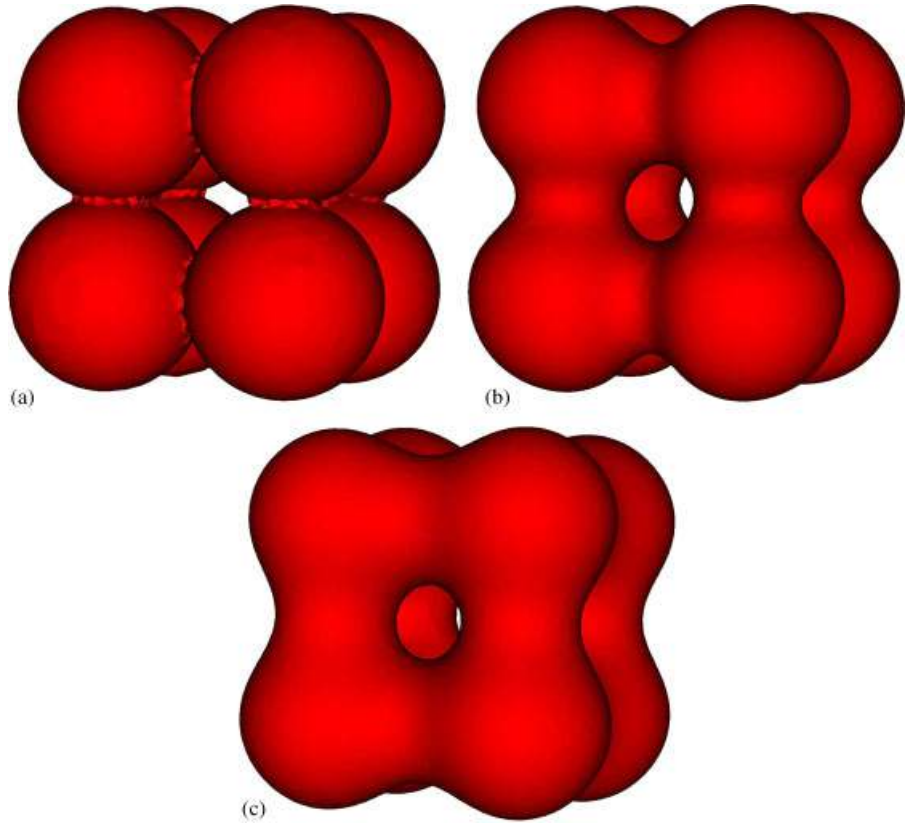

Figure 15. Change in 8 grains under surface diffusion (three-dimensional case, $\Delta t = 10^{-2}$, $C_0 = 10^{-7}$). (a) $t = 0$; (b) $t = 1$; and (c) $t = 5$.

toward an equilibrium state. The CPU time of this computation which involves 500 time steps, is of 2 h by using a parallel computing strategy on four cores (Intel Xeon 2.2 GHz processor).

5. CONCLUSION

Within the general context of the sintering process simulation, a finite element level set formulation of the surface diffusion problem has been proposed. The main difficulty induced by this approach, the dependence of the surface velocity on the fourth-order spatial derivative of the level set function, has been overcome by considering a mixed system in curvature/surface Laplacian of the curvature. This formulation induces implicitly a stabilization term Δv_n with an associated stabilization parameter depending on the time step. The resulting discretized formulation is shown to be stable in all our simulations. Several simulations have been carried out and analyzed in details. On one hand, convergence properties in shape and area conservation have been studied by considering several structured and unstructured mesh. The relevancy and accuracy of the developed numerical methodology have then been shown by comparing the simulations with analytical models (evolution of an ellipsoid surface, sintering of two grains). On the other hand, the large possibilities of the adopted approach (taking into account an 'arbitrary' number of grains without restrictions on their shape, in two or three dimensions, capturing automatically the closed porosity) have been exposed for the context of the sintering simulation.

The outlooks to this work are numerous. First of all, the simulation results involving two grains or more have to be confronted to experimental results. Such confrontations are complex to do, making necessary the choice of a reference material for the surface diffusion and the use of statistical methods to achieve the comparison. However, this step is mandatory to examine the

ability of the numerical simulation to help the scientist in controlling the final microstructure of a sintered material. Furthermore, as the aim of this work is precisely to develop a numerical tool for the sintering process simulation, the next steps in the development of this work are to take into account the different paths of matter transport. First, the grain-boundary diffusion which requires the description (by a level set function) of the boundary separating two particles. Second, the volume diffusion that introduces the mechanical response of the material to a given loading.

REFERENCES

1. Ashby MF. A first report on sintering diagrams. *Acta Metallurgica et Materialia* 1974; **22**(3):275–289.
2. Rahaman MN. *Ceramic Processing and Sintering*. Marcel Dekker Inc.: New York, 1995.
3. Bernoff AJ, Bertozzi AL, Witelski TP. Axisymmetric surface diffusion: dynamics and stability of self-similar pinch-off. *Journal of Statistical Physics* 1998; **93**(3–4):725–776.
4. Escher J, Mayer UF, Simonett G. The surface diffusion flow for immersed hypersurfaces. *SIAM Journal on Mathematical Analysis* 1998; **29**(6):1419–1433.
5. German RM, Lathrop JF. Simulation of spherical powder sintering by surface diffusion. *Journal of Materials Science* 1978; **13**(5):921–929.
6. Pan J, Cocks ACF, Kucherenko S. Finite element formulation of coupled grain-boundary and surface diffusion with grain-boundary migration. *Proceedings of the Royal Society A* 1997; **453**(1965):2161–2184.
7. Bouvard D, McMeeking RM. Deformation of interparticle necks by diffusion-controlled creep. *Journal of the American Ceramic Society* 1996; **79**(3):665–672.
8. Darcovich K, Shinagawa K, Walkowiak F. A three-dimensional dual-mechanism model of pore stability. *Materials Science and Engineering A* 2004; **373**(1–2):107–114.
9. Barrett JW, Garcke H, Nürnberg R. A parametric finite element method for fourth order geometric evolution equations. *Journal of Computational Physics* 2007; **222**(1):441–467.
10. Barrett JW, Garcke H, Nürnberg R. On the parametric finite element approximation of evolving hypersurfaces in $\mathbb{R}^3$. *Journal of Computational Physics* 2008; **227**(9):4281–4307.
11. Adalsteinsson D, Sethian JA. A level set approach to a unified model for etching, deposition, and lithography—III: redeposition, reemission, surface diffusion, and complex simulations. *Journal of Computational Physics* 1997; **138**(1):193–223.
12. Li Z, Zhao H, Gaoz H. A numerical study of electro-migration voiding by evolving level set functions on a fixed cartesian grid. *Journal of Computational Physics* 1999; **152**(1):281–304.
13. Chopp DL, Sethian JA. Motion by intrinsic Laplacian of curvature. *Interfaces and Free Boundaries* 1999; **1**(1):107–123.
14. Smereka P. Semi-implicit level set method for curvature and surface diffusion motion. *Journal of Scientific Computing* 2003; **19**(1–3):439–456.
15. Sethian JA. Level sets methods and fast marching methods. *Cambridge Monograph on Applied and Computational Mathematics*, vol. 3, 1999.
16. Osher S, Fedkiw F. Level set methods: an overview and some recent results. *Journal of Computational Physics* 2001; **169**(2):463–502.
17. Bruchon J, Digonnet H, Coupez T. Using a signed distance function for the simulation of metal forming processes: Formulation of the contact condition and mesh adaptation. From a Lagrangian approach to an Eulerian approach. *International Journal for Numerical Methods in Engineering* 2009; **78**(8):980–1008.
18. Ville L, Silva L, Coupez T. Convected level set method for the numerical simulation of fluid buckling. *International Journal for Numerical Methods in Engineering*. DOI: //dx.doi.org/10.1002/fld.2259.
19. Bernacki M, Chastel Y, Coupez T, Logé RE. Level set framework for the numerical modelling of primary recrystallization in polycrystalline materials. *Scripta Materialia* 2008; **58**(12):1129–1132.
20. Burger M, Hausser F, Stöcker C, Voigt A. A level-set approach to anisotropic flows with curvature regularization. *Journal of Computational Physics* 2007; **225**(1):183–205.
21. Bänsch E, Morin P, Nochetto RH. A finite element method for surface diffusion: the parametric case. *Journal of Computational Physics* 2005; **203**(1):321–343.
22. Marcellini P, Miller K. Elliptic versus parabolic regularization for the equation of prescribed mean curvature. *Journal of Differential Equations* 1997; **137**(1):1–53.
23. Digonnet H, Coupez T. Object-oriented programming for 'fast-and-easy' development of parallel applications in forming processes simulation. In *Second MIT Conference on Computational Fluid and Solid Mechanics*, Bathe KJ (ed.). Massachusset Institute. Elsevier: Amsterdam, 2003; 1922–1924.
24. Mesri Y, Digonnet H, Coupez T. Advanced parallel computing in material forming with CIMLib. *European Journal of Computational Mechanics* 2009; **18**(7–8):669–694.
25. Pan J, Kucherenko LH, Yeomans JA. A model for sintering of spherical particles of different sizes by solid state diffusion. *Acta Metallurgica et Materialia* 1998; **46**(13):4671–4690.
26. Martin CL, Bouvard D, Shima S. Study of particle rearrangement during powder compaction by discrete element method. *Journal of the Mechanics and Physics of Solids* 2003; **51**(4):667–693.